Detachment onset in MAST-U according to SOLPS-ITER

D. Moulton[1], B. Lipschultz[2], J. Harrison[1]

[1] *Culham Centre for Fusion Energy, Culham Science Centre, Abingdon, OX14 3DB, UK*

[2] *Department of Physics, University of York, Heslington, York, YO10 5DD, UK*

The pedestal pressure that can be obtained in H-mode is known to be inversely correlated with the electron density at the outer mid-plane separatrix [Dunne2017]. In order to maximise core performance whilst minimising target loads, it is therefore necessary to minimise the upstream separatrix density at which target detachment occurs. One promising means to do this is with a Super-X divertor, the first of which is currently being installed on MAST-Upgrade [Fishpool2013]. Here, we use the SOLPS-ITER code [Wiesen2015] to investigate the underlying physics behind detachment onset (i.e. the point in a density scan at which the target electron flux density starts to decrease as a function of the upstream density) in MAST-U.

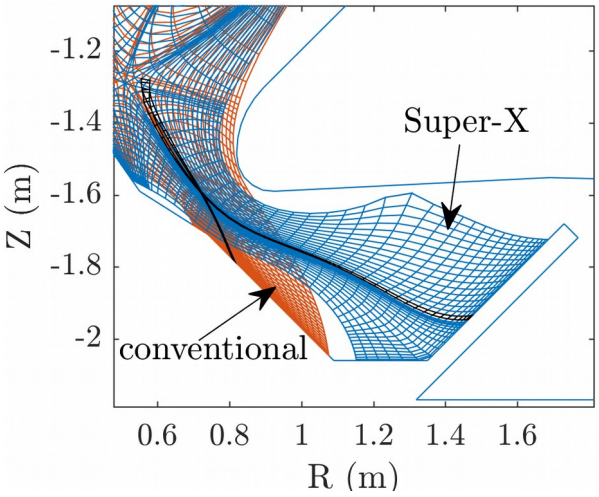

Figure 1: The numerical grids. The particular flux tubes analysed are outlined in black.

The grids used are shown in figure 1. Both grids were connected double null. The SOLPS-ITER code was run with drifts turned off, assuming zero current. The default set of neutral reactions was used [Kotov2008] and neutral-neutral collisions were turned off. The radial diffusivities above the X-point were set in order to achieve radial SOL widths of

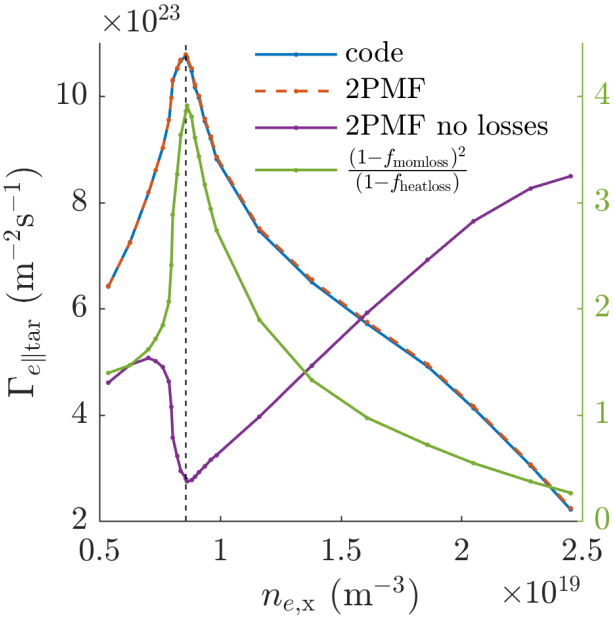

Figure 2: Parallel electron flux density at the target along the 3rd flux tube in the Super-X grid, as a function of the electron density at the X-point. Comparison to the 2PMF equation is also shown. See text for details.

λ_q,=6mm, λ_n =17mm, and λ_{Te}.=24mm, similar to values found in MAST H-mode [Kirk2004,Harrison2013,Thornton2014]. Below the X-point, we assumed 1 m^2s^{-1} for all radial diffusivities. The input power across the core-facing flux surface was set to 2.5 MW and the total pumping speed was 10.7 m^3s^{-1}, shared equally between upper and lower divertors (all simulations were top-bottom symmetric). As it will be on MAST-U, the strength of the D_2 puff at the inner mid-plane was varied in order to achieve a density scan. Intrinsic carbon impurities were included in the simulations, with a chemical sputtering yield of 3%. No extrinsic impurities were seeded in these simulations.

We analyse the third flux tube of the Super-X grid, for which the target heat flux density was maximum in the attached regime. Figure 2 shows the parallel electron flux density at the target, $\Gamma_{e\|tar}$, as a function of the electron density at the X-point, n_{ex}. To understand this rollover, we use the two-point model formulation (2PMF) equation for $\Gamma_{e\|tar}$ [Kotov2009,Stangeby2017]:

$$\Gamma_{e\|tar} = \frac{\gamma}{8m}\frac{p_{tot,u}^2}{q_{\|u}}\frac{(1-f_{momloss})^2}{1-f_{heatloss}}\frac{2}{1+\tau_{tar}/z_{tar}}\frac{4M_{tar}^2}{(1+M_{tar}^2)^2}\frac{B_u}{B_t} \quad , \qquad (1)$$

where each symbol is as defined in [Kotov2009] and [Stangeby2017] (in particular, $f_{momloss}$ and $f_{heatloss}$ are the fractions of total pressure and total heat flux, respectively, lost between the upstream end and the target end of a flux tube). 'Upstream' here is the entrance to the divertor. We see that the code value for $\Gamma_{e\|tar}$ and the 2PMF equation agree, demonstrating the correctness of equation (1). Importantly, equation (1) without the $(1-f_{momloss})^2/(1-f_{heatloss})$ loss term (purple line) does not correlate well with the rollover, while the $(1-f_{momloss})^2/(1-f_{heatloss})$ term (green line, right-hand axis) does. We conclude that losses along the flux tube drive the rollover in $\Gamma_{e\|ta}$.

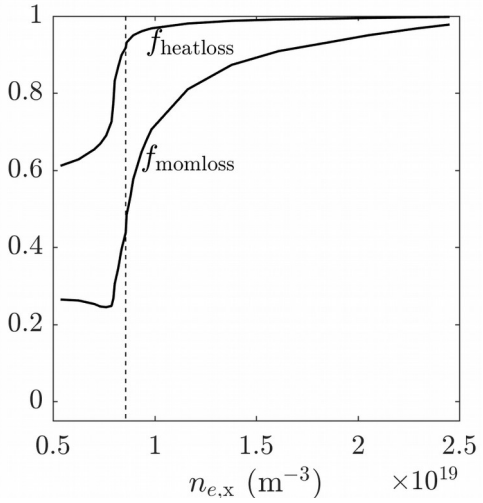

Figure 3: $f_{momloss}$ and $f_{heatloss}$ as a function of the X-point density

Analysing $f_{momloss}$ and $f_{heatloss}$ separately (figure 3), we see that almost all of the heat is exhausted from the flux tube before the rollover, at which point the increasing $f_{momloss}$ brings $\Gamma_{e\|tar}$ down with increasing upstream density. This is in line with simple heat balance models

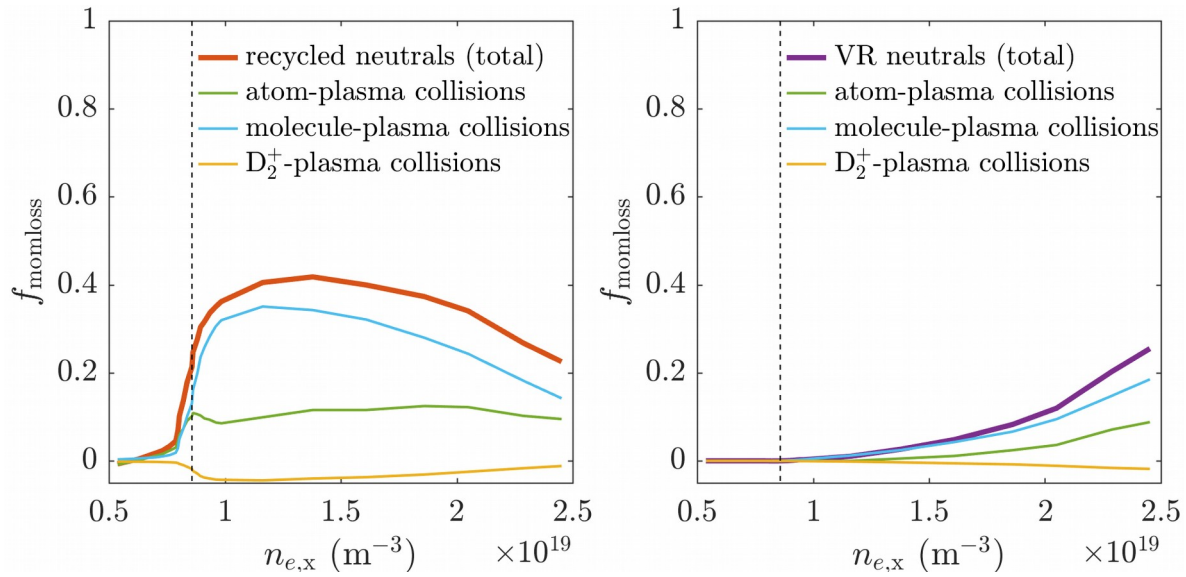

Figure 4: Decomposition of $f_{momloss}$ due to neutrals born as recycled molecules (left) and neutrals born as volumetrically recombined atoms (right). Further decomposition is shown by reaction type. Dashed line indicates the position of $\Gamma_{e\|tar}$ rollover.

where detachment onset is assumed to occur once all the heat has been exhausted [Lipschultz2016]. Further analysis of the neutral mechanisms which lead to plasma momentum loss (figure 4) shows that, at rollover, most of the neutral contribution to $f_{momloss}$ is due to molecules that are recycled from the targets after surface recombination of the ion target flux. It is not until much later in the density scan that neutrals born as atoms after volume recombination remove significant momentum. For both sources of neutrals, the dominant loss mechanism is via molecule-plasma collisions (primarily ion-molecule elastic collisions), similar to previously found in ASDEX-Upgrade simulations [Kotov2009]. This implies that volumetrically recombined neutrals remove most momentum after they have reflected from the target as D_2. Atom-plasma collisions (primarily charge exchange) play only a secondary role in momentum loss.

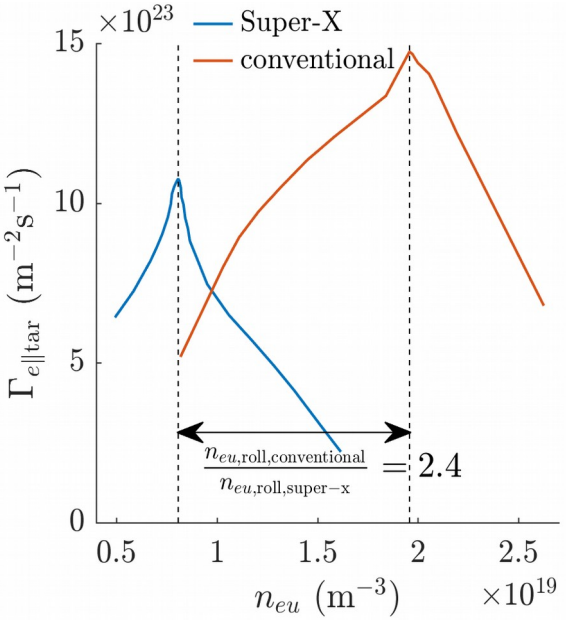

Figure 5: Rollover of $\Gamma_{e\|tar}$ for the Super-X and conventional grids shown in figure 1.

Figure 5 shows the rollover in $\Gamma_{e\|tar}$ for the two grids shown in figure 1. For a fair comparison, plots are made as a function of the electron density at the top of the flux tube rather than at the X-point. The upstream density at which rollover occurs is a factor 2.4 times greater in conventional than in Super-X. To understand why, we rearrange the 2PMF equations for the target electron temperature [Stangeby2017] at rollover for the conventional and Super-X grids, to give:

$$\frac{n_{eu,roll,conv}}{n_{eu,roll,super-x}} = \left[\frac{(\sqrt{m}/\gamma)_{conv}}{(\sqrt{m}/\gamma)_{super-x}} \frac{(1+\tau_u/z_u)_{super-x}}{(1+\tau_u/z_u)_{conv}} \sqrt{\frac{(1+\tau_{tar}/z_{tar})_{conv}}{(1+\tau_{tar}/z_{tar})_{super-x}}}\right] \times \left[\frac{T_{eu,super-x}}{T_{eu,conv}} \frac{q_{\|u,conv}}{q_{\|u,super-x}}\right] \times \left[\sqrt{\frac{T_{e,tar,super-x}}{T_{e,tar,conv}}}\right] \times \left[\frac{((1+M_{tar}^2)/M_{tar})_{conv}}{((1+M_{tar}^2)/M_{tar})_{super-x}}\right] \times \left[\frac{(1-f_{heatloss,conv})}{(1-f_{heatloss,super-x})}\right] \times \left[\frac{(1-f_{momloss,super-x})}{(1-f_{momloss,conv})}\right] \times \left[\frac{(B_u/B_{tar})_{super-x}}{(B_u/B_{tar})_{conv}}\right], \quad (2)$$

where parameters on the right hand side are given at rollover. Equation (2) is exact except for an assumption that all of the upstream pressure is static (which is well met in all simulations). In order, the values of each factor in square brackets are: 1.15, 1.05, 0.86, 0.99, 1.17, 1.06 and 1.88. A difference in the neutral pathways between the two configurations would manifest as a deviation from unity in the 3rd, 5th and 6th factors, i.e. a difference in the target temperatures and/or the loss factors. However, we do not see a significant deviation in any of the factors except the final factor, which is the ratio of the total flux expansion in Super-X compared to conventional. This suggests that, for these simulations, it is the increased total flux expansion in the Super-X (relative to the conventional, defined as the ratio of magnetic field strength upstream to that at the target), which is the primary cause of the decrease in the upstream density at which rollover occurs.

References

M. G. Dunne *et al*., Plasma Phys. Control. Fusion **59** 014017 (2017)
G. Fishpool *et al*., J. Nucl. Mater. **438** S536 (2013)
J. Harrison *et al*., J. Nucl. Mater **438** S375 (2013)
A. Kirk *et al*., Plasma Phys. Control. Fusion **46** 1591 (2004)
V. Kotov et al., Plasma Phys. Control. Fusion **50** 105012 (2008)
V. Kotov and D. Reiter, Plasma Phys. Control. Fusion **51** 115002 (2009)
B. Lipschultz *et al*., Nucl. Fusion **56** 056007 (2016)
P. C. Stangeby and C. Sang, Nucl. Fusion **57** 056007 (2017)
A. Thornton *et al*., Plasma Phys. Control. Fusion **56** 055008 (2014)
S. Wiesen *et al*., J. Nucl. Mater. **463** 480 (2015)

This work has been carried out within the framework of the EUROfusion Consortium and has received funding from the Euratom research and training programme 2014-2018 under grant agreement No 633053 and from the RCUK Energy Programme [grant number EP/P012450/1]. The views and opinions expressed herein do not necessarily reflect those of the European Commission.